

Ghost imaging in scattering media

Wenlin Gong, Pengli Zhang, Xia Shen, and Shensheng Han*
 Key Laboratory for Quantum Optics and Center for Cold Atom Physics,
 Shanghai Institute of Optics and Fine Mechanics,
 Chinese Academy of Sciences, Shanghai 201800, China
 (Dated: March 8, 2019)

Ghost imaging with thermal light in scattering media is investigated. We demonstrated experimentally for the first time that the image with high quality can still be obtained in the scattering media by ghost imaging. The scattering effect on the qualities of the images for conventional imaging and ghost imaging is analysed theoretically. Its potential applications are also discussed.

PACS numbers: 42.68.Mj, 42.50.Dv, 42.62.Be, 42.50.Ar, 42.30.Kq

I. INTRODUCTION

Multiple scattering has a great effect on the qualities of images and the transmission of information. The information will be decayed and the images suffer reduced resolution and contrast because of multiple scattering. For example, the measurement of the laser radar [1], satellite communications [2], the propagation and imaging of light in the atmosphere [3], neutron imaging [4] and the imaging and diagnosis in life and medical science [5]. So the imaging in strong scattering media is always a great problem and presents a key challenge for the research of better imaging method and technique.

In clinic applications, the most common imaging modalities include ultrasound imaging, X-ray computed tomography(CT), and magnetic resonance imaging (MRI) [5, 6]. As the development of imaging technology, optical imaging is becoming an increasing interesting method for the imaging in biological tissue. By now most imaging methods are obtained by using the gating techniques. Such as confocal imaging, spatial filtering, optical coherence tomography (OCT), Mueller optical coherence tomography, Diffuse optical tomography (DOT), Photoacoustic tomography (PAT), Ultrasound-Modulated optical tomograph (UOT) and so on [6, 7, 8, 9, 10, 11, 12, 13, 14]. Although the quality of the image has a great increase by these techniques, there is still lots of problems which are urgent to be solved.

The first two-photon imaging experiment with entangled source was demonstrated by Pittman *etal.* in 1995 [15], which shew that we could obtain a nonlocal image by transmitting pairs of photons through a test and a reference path. In 2004, the theories and experiments also demonstrated that the ghost imaging could also be obtained with thermal light [16, 17, 18, 19, 20, 21]. Recently we find that the quality of the ghost imaging is determined by both the reference path and the test path [22]. Because multiple scattering only degrades the imaging quality in the test path, whereas there is no multiple scattering in the reference path. By correlation measure-

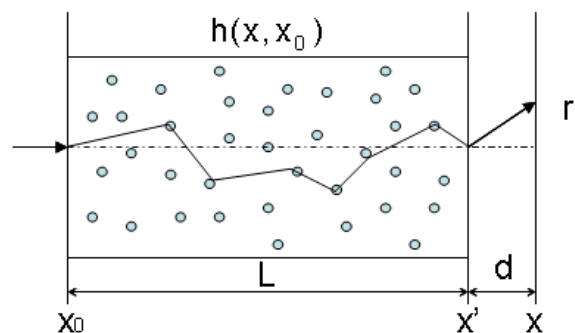


FIG. 1: Schematic diagram for the light transmitting in a scattering media.

ment, we may get a image with much better quality than the image obtained by detection in a single path.

II. THEORY AND ANALYSIS

Schematic diagram for the light transmitting in a scattering media is shown in Fig. 1. In the theory of linear systems [24], the light field $E(x)$ in the plane x is the convolution of the light field $E(x_0)$ in the plane x_0 and the impulse response function $h(x, x_0)$.

$$E(x) = \int dx_0 E(x_0) h(x, x_0). \quad (1)$$

For light transmission in scattering media, the light field in the position x is the linear superposition the incident light and the scattering light.

$$E(x) = \alpha \int dx_0 E(x_0) h_{in}(x, x_0) + \beta \int dx_0 E(x_0) h_{sca}(x, x_0), \quad (2)$$

$$|\alpha|^2 + |\beta|^2 = 1. \quad (3)$$

where $h_{in}(x, x_0)$ is the impulse response function with no scattering media, and $h_{sca}(x, x_0)$ is the impulse response

*Electronic address: sshan@mail.shcnc.ac.cn

function from the plane x_0 to the plane x because of the interactions of multiple scattering, and α, β are the probability amplitudes of the incident light and the scattering light, respectively. From Eqs. (1)-(3), we have

$$h(x, x_0) = \alpha h_{in}(x, x_0) + \beta h_{sca}(x, x_0). \quad (4)$$

The probability distribution function in the scattering media is called point scattering function. The impulse response function $h_{sca}(x, x_0)$ has close contact with the point scattering function which is Dirac delta function when there is no scattering media. However, in the scattering media, it is a spread function with a broadening length, and generally the point scattering function has two forms: Lorentzian-shaped and Gaussian-shaped distribution [34, 35]. In multiple scattering Mie theory [25, 26, 27], both of probability amplitudes α, β are depending on the diameter size of the particle D , the wavelength of the incident light λ , the concentration of the suspended particles w and the effective length of the scattering media L . According to the experiments and theories [28, 29, 30, 31, 32, 33, 34, 35], we have

$$\alpha = \alpha(D, \lambda, w, L) \propto \frac{\lambda^{b_\alpha}}{D^{a_\alpha} w^{c_\alpha} L^{d_\alpha}}, \quad (5a)$$

$$\beta = \beta(D, \lambda, w, L) \propto \frac{D^{a_\beta} w^{c_\beta} L^{d_\beta}}{\lambda^{b_\beta}}, \quad (5b)$$

$$h_{sca}(x, x_0) \propto P(x', x_0)_{(L+d)_A} h(x, x_0)_{(L+d)_A}, \quad (5c)$$

$$h(x, x_0)_{(L+d)_A} = h_{in}(x', x_0)_L h_{in}(x, x')_{L+d}, \quad (5d)$$

$$P(x', x_0)_{(L+d)_A} = \left[\frac{2}{\pi \Delta x_{(L+d)_A}^2} \right]^{1/4} \times \exp \left\{ - \left(\frac{x' - x_0}{\Delta x_{(L+d)_A}} \right)^2 \right\}, \quad (5e)$$

$$\Delta x_{(L+d)_A} \propto \frac{D^{a_x} w^{c_x} (L+d)_A^{d_x}}{\lambda^{b_x}}, \quad (5f)$$

$$\int |P(x', x_0)_{(L+d)_A}|^2 dx' = 1. \quad (5g)$$

where $P(x', x_0)_{(L+d)_A}$ is the probability amplitude. $\Delta x_{(L+d)_A}$ is the broadening length because of the interactions of multiple scattering, and it becomes wider with the increase of the scattering length. With the increase of the broadening length, the frequency spectrum of the optical transfer function becomes narrower, which is the main reason leading to the degradation of the quality of information transmission and image [32, 33]. $(L+d)_A$ is the approximated distance between the scattering point and the detection plane, and it is not equal to the geometric distance for forward scattering [34]. We suppose point

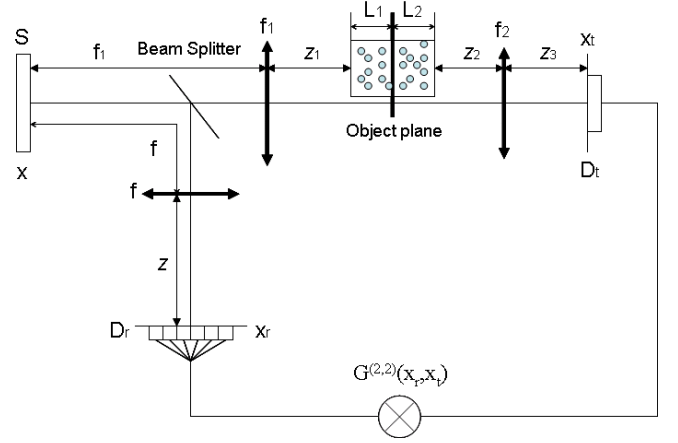


FIG. 2: Scheme for ghost imaging with thermal light in the scattering media.

scattering function is Gaussian-shaped distribution, and the impulse response function of the multiple scattering is assumed as $h(x, x_0)_{(L+d)_A}$ without considering the absorption of the scattering media. All the coefficients in Eq. (5) should be determined by specific experimental conditions.

The scheme for ghost imaging with thermal light in the scattering media is shown in Fig. 2. The light source S , first propagates through a beam splitter, then is divided into a test and a reference path. In the test path, the light propagates through a single lens of focal length f_1 , the scattering media and then to the detector D_t . In the reference path, the light propagates through a single lens of focal length f then to an array of pixel detector D_r .

By optical coherence theory [16, 23], we can obtain the correlation function of intensity fluctuations between the detectors:

$$\Delta G^{(2,2)}(x_r, x_t) = \langle \Delta I_r(x_r) \Delta I_t(x_t) \rangle = |\Gamma(x_r, x_t)|^2, \quad (6a)$$

$$\Gamma(x_r, x_t) = \int dx_1 \int dx_2 G^{(1,1)}(x_1, x_2) h_r^*(x_r, x_1) \times h_t(x_t, x_2). \quad (6b)$$

where $\Gamma(x_r, x_t)$ is the first-order cross-correlation function of two different points from the test and reference paths.

Suppose the light source is fully spatially incoherent, then

$$G^{(1,1)}(x_1, x_2) = I_0 \delta(x_1 - x_2). \quad (7)$$

where I_0 is a constant, and $\delta(x)$ is the Dirac delta function. Under the paraxial and small angle approximation, and when the effective apertures of the lenses in the optical system are large enough, the impulse response function of the reference system is

$$h_r(x_r, x_1) \propto \exp \left\{ \frac{j\pi}{\lambda f} \left(1 - \frac{z}{f} \right) x_1^2 - \frac{2j\pi}{\lambda f} x_r x_1 \right\}. \quad (8)$$

$f_2, z_2 + L_2, z_3$ obey the Lens Law

$$\frac{1}{z_2 + L_2} + \frac{1}{z_3} = \frac{1}{f_2}. \quad (9)$$

when

$$\frac{f_1}{f} = \frac{z_2 + L_2}{z_3}. \quad (10)$$

The impulse response function of the test system is

$$\begin{aligned} h(x_t, x_2) \propto & \int dx' [\alpha_1 \exp \left\{ -\frac{2j\pi}{\lambda f_1} x' x_2 \right\} + \beta_1 \int dx'_2 \\ & \times P(x', x'_2)_{L_{1A}} \exp \left\{ \frac{j\pi}{\lambda L_1} (x' - x'_2)^2 - \frac{2j\pi}{\lambda f_1} x'_2 x_2 \right\}] \\ & \times t(x') C(x') \exp \left\{ \frac{j\pi}{\lambda f_1} \left(1 - \frac{z_1 + L_1}{f_1}\right) x_2^2 \right\} \end{aligned} \quad (11a)$$

$$\begin{aligned} C(x) = & [\alpha_2 \delta(x + \frac{f_1}{f} x_t) + \beta_2 P(-\frac{f_1}{f} x_t, x)_{(L_2+z_2)A} \\ & \times \exp \left\{ \frac{j\pi}{\lambda L_2} \left(\frac{f_1}{f} x_t + x\right)^2 \right\}]. \end{aligned} \quad (11b)$$

Substituting Eqs. (7) and (9)-(11b) into Eq. (6b), we can get the intensity distribution in the test path

$$\begin{aligned} I(x_t) \propto & \int dx' \int dx'' t(x') t^*(x'') \{ |\alpha_1|^2 \delta(x' - x'') \\ & + 2P(x', x'')_{L_{1A}} \text{Re}[\alpha_1^* \beta_1 \exp \left\{ \frac{j\pi}{\lambda L_1} (x' - x'')^2 \right\}] \\ & + |\beta_1|^2 \int dx'_2 \exp \left\{ \frac{j\pi}{\lambda L_1} [(x' - x'_2)^2 - (x'' - x'_2)^2] \right\} \\ & \times P(x', x'_2)_{L_{1A}} P(x'', x'_2)_{L_{1A}} \} C(x') C^*(x''). \end{aligned} \quad (12)$$

Eq. (12) describes the images in the scattering media for conventional imaging system. When

$$\frac{1 - \frac{z}{f}}{f} = \frac{1 - \frac{z_1 + L_1}{f_1}}{f_1}. \quad (13)$$

substituting Eqs. (7)-(11b) and (13) into Eq. (6), we can obtain the correlation function of intensity fluctuations

$$\begin{aligned} \Delta G^{(2)}(x_r, x_t) \propto & |\alpha_1 \alpha_2 C_1 + \alpha_1 \beta_2 C_2 \\ & + \beta_1 \alpha_2 C_3 + \beta_1 \beta_2 C_4|^2, \end{aligned} \quad (14a)$$

$$C_1 = \delta(x_r + x_t) t(-\frac{f_1}{f} x_t), \quad (14b)$$

$$\begin{aligned} C_2 = & t(\frac{f_1}{f} x_r) P(-\frac{f_1}{f} x_t, \frac{f_1}{f} x_r)_{(L_2+z_2)A} \\ & \times \exp \left\{ \frac{j\pi f_1^2}{\lambda L_2 f^2} (x_t + x_r)^2 \right\}, \end{aligned} \quad (14c)$$

$$\begin{aligned} C_3 = & t(-\frac{f_1}{f} x_t) P(-\frac{f_1}{f} x_t, \frac{f_1}{f} x_r)_{L_{1A}} \\ & \times \exp \left\{ \frac{j\pi f_1^2}{\lambda L_1 f^2} (x_r + x_t)^2 \right\}, \end{aligned} \quad (14d)$$

$$\begin{aligned} C_4 = & \int dx' t(x') P(x', \frac{f_1}{f} x_r)_{L_{1A}} P(-\frac{f_1}{f} x_t, x')_{(L_2+z_2)A} \\ & \times \exp \left\{ \frac{j\pi}{\lambda L_1} (x' - \frac{f_1}{f} x_r)^2 + \frac{j\pi}{\lambda L_2} \left(\frac{f_1}{f} x_t + x'\right)^2 \right\} \end{aligned} \quad (14e)$$

The ghost imaging in the scattering media is described by the Eqs. (14a)-(14e). And it is a image with high quality for C_1 and C_2 , which implies we can still get a image with high resolution by ghost imaging in the scattering media.

From Eqs. (14a)-(14e), if the test detector is an array of pixel detector, and $x_t = -x_r$, after some calculation, then

$$\begin{aligned} \Delta G^{(2)}(x_r, -x_r) \propto & \left\{ \alpha_1 \alpha_2 + \alpha_1 \beta_2 \left[\frac{2}{\pi \Delta x_{(L_2+z_2)A}^2} \right]^{1/4} \right. \\ & \left. + \beta_1 \alpha_2 \left[\frac{2}{\pi \Delta x_{L_{1A}}^2} \right]^{1/4} \right\} t(\frac{f_1}{f} x_r) + \beta_1 \beta_2 C_4 \Big|^2 \end{aligned} \quad (15)$$

if the test detector is a bucket detector, then

$$\begin{aligned} \Delta G^{(2)}(x_r) \propto & \int dx_t |\alpha_1 \alpha_2 C_1 + \alpha_1 \beta_2 C_2 \\ & + \beta_1 \alpha_2 C_3 + \beta_1 \beta_2 C_4|^2. \end{aligned} \quad (16)$$

Eqs. (15) and (16) represent the ghost imaging when the test detector is an array of pixel detector or a bucket detector, respectively.

For $L_1 = 0$, there is only multiple scattering between the object plane and the test detector, then we have $|\alpha_1| = 1, \beta_1 = 0$. By Eq. (12), the intensity distribution in the test path is

$$I_t(x_t) \propto (|\alpha_2|^2 + 2C_{5t}) \left| t(-\frac{f_1}{f} x_t) \right|^2 + C_{6t} |\beta_2|^2, \quad (17a)$$

$$C_{5t} = \left[\frac{2}{\pi \Delta x_{(L_2+z_2)A}^2} \right]^{1/4} \text{Re}[\alpha_2^* \beta_2], \quad (17b)$$

$$\begin{aligned} C_{6t} = & \int dx' |t(x')|^2 \left| P(-\frac{f_1}{f} x_t, x')_{(L_2+z_2)A} \right|^2 \\ & = \left[\frac{2}{\pi \Delta x_{(L_2+z_2)A}^2} \right]^{1/2} \int dx' |t(x')|^2 \\ & \times \exp \left\{ -\frac{2}{\Delta x_{(L_2+z_2)A}^2} \left(x' + \frac{f_1}{f} x_t\right)^2 \right\}. \end{aligned} \quad (17c)$$

the last term in Eq. (17a) is the main reason leading to the decrease of the resolution of the image when there

is multiple scattering between the object plane and the detector. With the increase of β_2 (and the decrease of the probability amplitude α_2), the resolution of the image will be further degraded.

Form Eq. (15), when the test detector is an array of pixel detector, after some calculation, then

$$\Delta G^{(2)}(x_r, -x_r) \propto \left| \alpha_2 + \beta_2 \left[\frac{2}{\pi \Delta x_{(L_2+z_2)A}^2} \right]^{1/4} \right|^2 \times \left| t\left(\frac{f_1}{f}x_r\right) \right|^2. \quad (18)$$

if the test detector is a bucket detector, By Eq. (16), then

$$\Delta G^{(2)}(x_r) \propto (|\alpha_2|^2 + 2C_5 + C_6 |\beta_2|^2) \left| t\left(\frac{f_1}{f}x_r\right) \right|^2, \quad (19a)$$

$$C_5 = \left[\frac{2}{\pi \Delta x_{(L_2+z_2)A}^2} \right]^{1/4} \text{Re}[\alpha_2^* \beta_2], \quad (19b)$$

$$C_6 = \int dx_t \left| P\left(-\frac{f_1}{f}x_t, \frac{f_1}{f}x_r\right)_{(L_2+z_2)A} \right|^2 \sim 1. \quad (19c)$$

from Eqs. (18)-(19c), we find that whether the test detector is an array of pixel detector or a bucket detector, the resolution of the ghost imaging will not be reduced even though there is multiple scattering between the object plane and the test detector.

For $L_2 = 0$, there is only multiple scattering between the source and the object plane, then we can gain $|\alpha_2| = 1, \beta_2 = 0$. By Eq. (12), the intensity distribution in the test path is

$$I_t(x_t) \propto (|\alpha_1|^2 + 2C_{7t} + C_{8t} |\beta_1|^2) \left| t\left(-\frac{f_1}{f}x_t\right) \right|^2, \quad (20a)$$

$$C_{7t} = \left[\frac{2}{\pi \Delta x_{L_{1A}}^2} \right]^{1/4} \text{Re}[\alpha_1^* \beta_1], \quad (20b)$$

$$C_{8t} = \int dx'_2 \left| P\left(-\frac{f_1}{f}x_t, x'_2\right)_{L_{1A}} \right|^2 \sim 1. \quad (20c)$$

From Eqs. (20a)-(20c), we find that the multiple scattering between the source and the object plane has no effect on the quality of the image.

From Eq. (15), when the test detector is an array of pixel detector, after some calculation, then

$$\Delta G^{(2)}(x_r, -x_r) \propto \left| \alpha_1 + \beta_1 \left[\frac{2}{\pi \Delta x_{L_{1A}}^2} \right]^{1/4} \right|^2 \times \left| t\left(\frac{f_1}{f}x_r\right) \right|^2. \quad (21)$$

which reveals that we can still obtain a image with high quality when the test detector is an array of pixel detector even if there is multiple scattering between the source and the object plane.

if the test detector is a bucket detector, By Eq. (16), then

$$\Delta G^{(2)}(x_r) \propto (|\alpha_1|^2 + 2C_7) \left| t\left(\frac{f_1}{f}x_r\right) \right|^2 + C_8 |\beta_1|^2, \quad (22a)$$

$$C_{7t} = \left[\frac{2}{\pi \Delta x_{L_{1A}}^2} \right]^{1/4} \text{Re}[\alpha_1^* \beta_1], \quad (22b)$$

$$C_8 = \int dx_t \left| t\left(-\frac{f_1}{f}x_t\right) P\left(-\frac{f_1}{f}x_t, \frac{f_1}{f}x_r\right)_{L_{1A}} \right|^2 = \left[\frac{2}{\pi \Delta x_{L_{1A}}^2} \right]^{1/2} \int dx_t \left| t\left(-\frac{f_1}{f}x_t\right) \right|^2 \times \exp \left\{ -\frac{2f_1^2}{\Delta x_{L_{1A}}^2 f^2} (x_t + x_r)^2 \right\}. \quad (22c)$$

where C_8 is the main factor leading to the decrease of the resolution of the image. $f_1 > f$ is helpful to improve the resolution of the image.

Figs. 3-5 present numerical results of imaging a single slit in scattering media based on Eqs. (12) and (15)-(16) (in which we take $\lambda=532\text{nm}$, $f_1=400\text{mm}$, $f=250\text{mm}$, the single slit width $a=0.2\text{mm}$). From Fig. 3(a), as the increase of L_2 , the resolutions of the images will decrease obviously for the conventional imaging. The resolutions of the images also reduce rapidly with the increase of the broadening length Δx_2 and the decrease of the probability amplitude α_2 when the object is fixed in the position of $L_1=0\text{mm}$, $L_2=100\text{mm}$ (Fig. 3(b), (c)), which accord with the results described by the Eqs (17a)-(17c).

Fig. 4 shows the numerical results when the position of the object in the scattering media is shifted. we can find that when the test detector is an array of pixel detector, multiple scattering has no effect on the resolution of the ghost imaging. And the resolution of the images also does not be significantly influenced when the test detector is a bucket detector.

Results shown in Figs. 5 reveals that the resolution of the ghost imaging doesn't reduce as the degradation of the probability amplitude α_2 when there is multiple scattering between the object plane and the test detector, whereas it will decrease slightly when there is multiple scattering between the object plane and the source.

III. EXPERIMENT

In the experiment, we prepare a suspension liquid which is composed by emulsion polymerization particles with particle diameter $D=4.96\mu\text{m}$ and the solution NaCl with the density $\rho=1.19\text{ g/cm}^3$. The liquid can

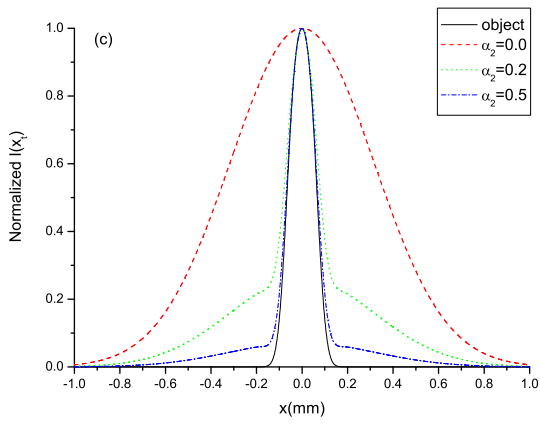
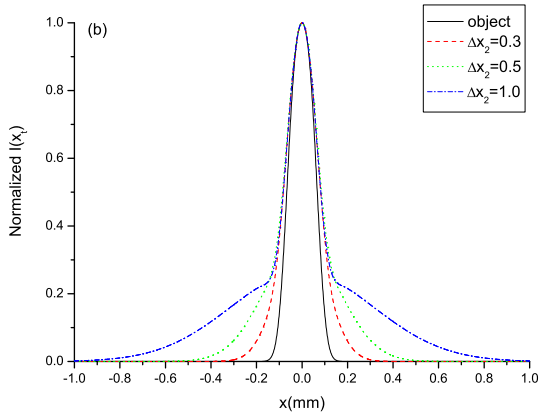
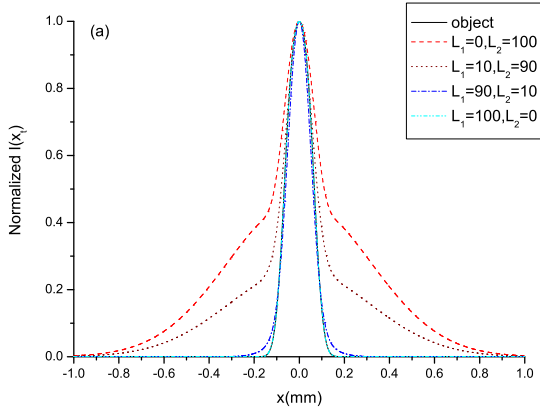


FIG. 3: Factors which have the effect on the qualities of the images for conventional imaging. (a). Images of a single slit at different positions in the scattering media; (b). Images of a single slit for different broadening length Δx_2 when $L_1=0\text{mm}$, $L_2=100\text{mm}$ and $\alpha_2=0.2$; (c). Images of a single slit for different probability amplitude α_2 when $L_1=0\text{mm}$, $L_2=100\text{mm}$ and the broadening length $\Delta x_2=1.0$.

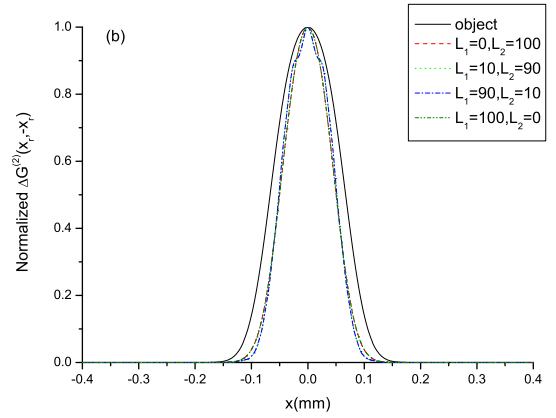
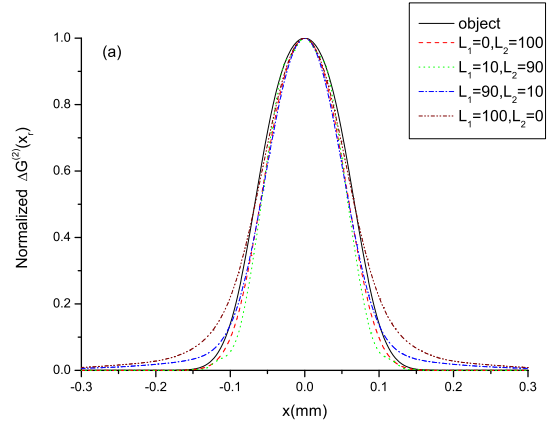
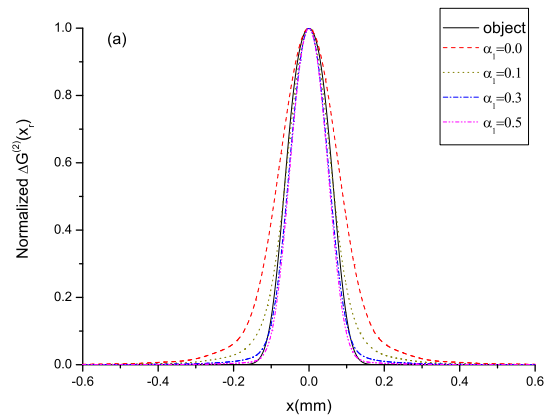


FIG. 4: Relationship between the resolution of the ghost imaging and the position of the object in scattering media. (a). the test detector is a bucket detector; and (b). the test detector is an array of pixel detector.



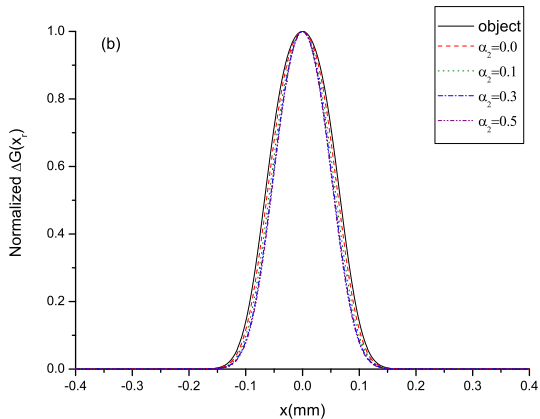


FIG. 5: Relationship between the resolution of the ghost imaging and the probability amplitude α_2 . (a). $L_1=100\text{mm}$, $L_2=0\text{mm}$ and the broadening length $\Delta x_1=1.0$; (b). $L_1=0\text{mm}$, $L_2=100\text{mm}$ and the broadening length $\Delta x_2=1.0$.

be considered as high multiple scattering media. And we take $\lambda=532\text{nm}$, $f_1=400\text{mm}$, $f=250\text{mm}$, $z=250\text{mm}$, $z_1=400\text{mm}$, $z_2=390\text{mm}$, $z_3=243.8\text{mm}$.

Images shown in Figs. 6(a1)-(a4), (b1)-(b4), and (c1)-(c4) are the experimental results of the object (**‘zhong’** ring) for conventional imaging and its ghost imaging when the object is at different positions in the scattering media, respectively.

Form Fig. 6, for conventional imaging the qualities of the images will reduce as the increase of the length L_2 of the scattering media, whereas their qualities don't degrade for ghost imaging when the test detector is an array of pixel detector, which accords with the theoretical results discussed above. And the resolutions of the images also change as the trend described in Figs. 4(a) and 5(a) when the test detector is a bucket detector. However, when the test detector is a bucket detector, the visibility of the ghost imaging will reduce as the increase of the length L_1 in the scattering media.

IV. DISCUSSION AND INCLUSION

For conventional imaging, the multiple scattering between the object plane and the detector is the main reason leading to the degradation of the qualities of the images, whereas it has no effect on the qualities of the ghost imaging whether the test detector is an array of pixel detector or a bucket detector, we can always obtain images with high qualities in the scattering media when the test detector is an array of pixel detector. However, as the multiple scattering between the source and the object plane is increased, although the resolution of the image does not be significantly influenced when the test detector is a bucket detector, the visibility of the image will

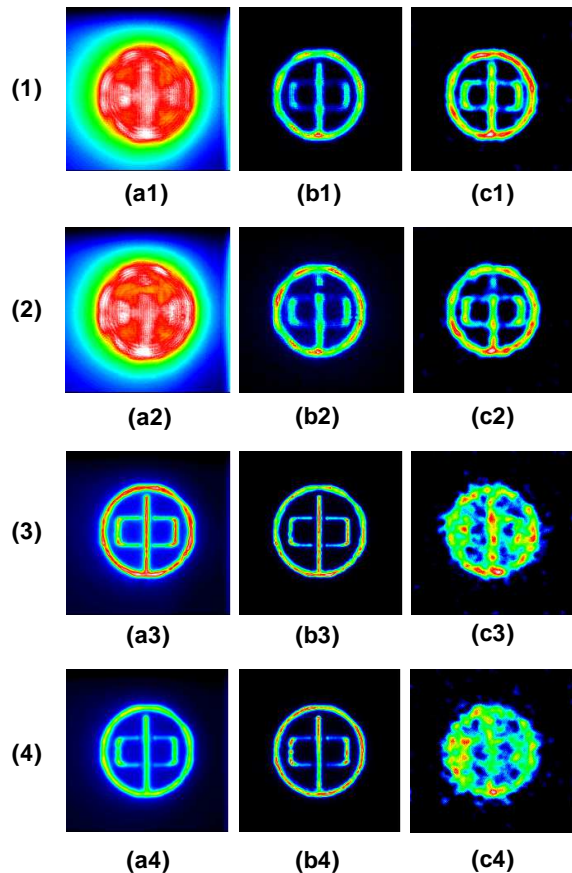


FIG. 6: Images of the aperture (**‘zhong’** ring) when the object is fixed in the different position of the scattering media. (1). $L_1=0\text{mm}$, $L_2=55\text{mm}$; (2). $L_1=5\text{mm}$, $L_2=50\text{mm}$; (3). $L_1=50\text{mm}$, $L_2=5\text{mm}$; and (4). $L_1=55\text{mm}$, $L_2=0\text{mm}$. (a1)-a(4). the conventional imaging; (b1)-(b4). ghost imaging with an array of pixel detector in the test path; (c1)-(c4). ghost imaging with a bucket detector in the test path.

reduce rapidly, because the multiple scattering leads to a decrease of the correlation between the test and reference paths. Generally speaking, with ghost imaging method, we can always obtain a image with much better quality on the base of the image obtained by a novel conventional imaging technique with thermal light.

In medical science, in order to avoid ionizing radiation of X-ray, optical photons provides nonionizing and safe radiation for medical applications. Recently there has been increasing interest in the field of the imaging, test and diagnosis of the biological tissues with the infrared and the near infrared light [6, 10, 14]. Because the near infrared light around 700-nm wavelength can penetrate several centimeters into biological tissue [14]. But several factors still limit the imaging quality. Because most biological tissues are characterized by strong optical scattering and hence are referred to as scattering media or turbid media. The images suffer reduced resolution and

contrast due to multiple scattering, which leads to a low efficiency and accuracy of diagnosis and a difficulty of analysis in medical science. So the diffusion-like behavior of light in biological tissue presents a key challenge for optical imaging. The ghost imaging discussed here may solve the problems about the low quality of the imaging in biological tissues.

In conclusion, we have shown that the images with high qualities in a scattering media can still be obtained by the correlation measurement of the intensity fluctuations when the test detector is an array of pixel detector, which will be very useful for the imaging and diagnosis in medical science. Otherwise, although there is multiple

scattering between the object plane and the test detector, we can always obtain images with high qualities whether the test detector is an array of pixel detector or a bucket detector by ghost imaging method. Furthermore, as the multiple scattering between the source and the object plane increased, the resolutions of the images do not be significantly influenced, but the visibility of the images will reduce rapidly when the test detector is a bucket detector.

The work was partly supported by the Hi-Tech Research and Development Program of China, Project No. 2006AA12Z115, and Shanghai Fundamental Research Project, Project No. 06JC14069.

-
- [1] G. W. Kamerman, Proc. SPIE, **4377**, 126-131 (2001).
- [2] H. G. Booker, and D. C. Miller, Journal of Atmospheric and Terrestrial Physics, **42**, 3 (1980).
- [3] T. S. McKechnie, J. Opt. Soc. Am. A, **8**, 2 (1991).
- [4] Raine D. A. , and Brenizer J. S. Materials evaluation, **55**, 1174 (1997).
- [5] K. P. Maher, J. F. Malone, and Brain Chance, Contemporary Physics, **38**, 131 (1997).
- [6] Lihong V. Wang and Hsin-i Wu, Biomedical optics: principle and imaging, (2007).
- [7] A. Yodh, and B. Chance, Phys. Today, **48**, 34 (1995).
- [8] S. R. Arridge, M. Cope, and D. T. Depty, Phys. Med. Biol. **37**, 1531 (1992).
- [9] S. R. Arridge, Topical Review, R41-93 (1999).
- [10] Sachin V. patwardhan, and Joseph P. Culver, J. Biomed. Opt. **13**(1), 011009 (2008).
- [11] J. C. Hebden, S. R. Arridge, M. Cope, and D. T. Depty, Phys. Med. Biol. **42**, 825 (1997).
- [12] B. Chance and R. R. Alfano, Proc. SPIE, 2389 (1995).
- [13] M. Laubscher, M. Ducros, B. Karamata, Opt. Exp. **10**, 9 (2002)
- [14] Brian C. Wilson, Eva M. Sevick, Michael S. Patterson, and Britton Chance, Proceedings of the IEEE. **80**, 6 (1992).
- [15] T. B. Pittman, Y. H. Shih, D. V. Strelakov, and A. V. Sergienko, Phys. Rev. A. **52**. R3429 (1995).
- [16] J. Cheng and S. Han, Phys. Rev. Lett. **92**. 093903 (2004).
- [17] A. Gatti, E. Brambilla, M. Bache, and L. A. Lugiato, Phys. Rev. A. **70**. 013802 (2004).
- [18] A. Gatti, E. Brambilla, M. Bache, and L. A. Lugiato, Phys. Rev. Lett. **93**. 093602 (2004).
- [19] A. Valencia, G. Scarcelli, M. D'Angelo, and Y. Shih, Phys. Rev. Lett. **94**. 063601 (2005).
- [20] R. S. Bennink, S. J. Bentley, and R. W. Boyd, Phys. Rev. Lett. **89**. 113601 (2002).
- [21] L. Basano and P. Ottonello, Appl. Phys. Lett. **89**, 091109 (2006).
- [22] Pengli Zhang, Wenlin Gong, Xia Shen, and Shensheng Han, arXiv. Quantum-ph/0804.0575 (2008).
- [23] R. J. Glauber, Phys. Rev. **130**, 2529 (1963).
- [24] J. W. Goodman, Introduction to Fourier optics (1976).
- [25] G. Mie, Ann. Phys. **330**, 377 (1908).
- [26] D. Toubanc, Appl. Opt. **35**, 3270 (1996).
- [27] S. K. Sharma, and A. K. Roy, J. Quant. Spectrosc. Radiat. Transfer. **64**, 327 (2000).
- [28] Jessica C. Ramella-Roman, Scott A. Prael, and Steven L. Jacques, Opt. Exp. **13**, 25 (2005).
- [29] Milun J. Rakovic and George W. Kattawar, Appl. opt. **37**, 15 (1999).
- [30] A. A. M. Mustafa and Daphne F. Jackson, Phys. Med. Biol. **26**, 461 (1981).
- [31] J. S. Faulkner and Eva A. Horvath, Phys. Rev. B. **44**, 8467 (1991).
- [32] W. H. Wells, J. Opt. Soc. Am. **59**, 6 (1969).
- [33] H. T. Yura, Appl. opt. **10**, 1 (1971).
- [34] Rene Hassanein, Eberhard Lehmann, and Peter Vontobel, Nucl. Ins. Meth. Phys. Res. A. **542**, 353 (2005).
- [35] P. N. Segre and P. N. Pusey, Phys. Rev. Lett. **77**, 4 (1996).